An Induced Voltage Source Model for Capacitive Power Transfer

Shiying Wang, Junrui Liang, Haoyu Wang, Minfan Fu
School of Information Science and Technology
ShanghaiTech University, Shanghai, China.
Email: fumf@shanghaitech.edu.cn

***Abstract*—Capacitive power transfer has been investigated as a constructive and significant alternative to the conventional inductive power transfer. It utilizes high-frequency electric field to realize wireless power transfer. However, the capacitive coupler is usually modeled by six coupling-dependent mutual capacitances. This model is hard for resonance analysis under the coupling variation. This paper explores an induced voltage source model for the capacitive coupler. It uses the two coupling-independent self-capacitances and a pair of induced voltage sources to represent the original six coupling-dependent capacitances. Such kind of modeling can well deal with the coupling variation and dramatically simplifies the resonance analysis. Both the finite-element-based simulation by Maxwell and real experiments are used to verify the proposed model. The results show that the self-capacitances are coupling-independent.**

***Index Terms*—Capacitive power transfer, Induced voltage source model**

I. Introduction

Capacitive power transfer (CPT) and inductive power transfer (IPT) are two effective method to transfer power from the transmitter (TX) to the receiver (RX) without direct contacts, which can be applied in the charge of portable devices and electric vehicles [1]–[7]. IPT technology has been investigated intensively and is a relative mature wireless power transfer (WPT) technology. However, IPT has an inherent disadvantage that is sensitive to nearby conductive object, and the system efficiency may decrease dramatically [8]. Therefore, as an alternative solution of WPT technology, CPT has drawn wide attention recently, due to its several unique advantages, such its low cost, no need of heavy magnetic cores, and the ability to transfer energy through metal barriers [9]–[11]. Based on electric field coupling, a CPT system usually needs a capacitive coupler to build a complete AC current loop. The capacitive coupler usually has four plates, e.g., two for the TX and two for the RX. From a physical point of view, there are totally six mutual capacitors. In most published works, the couplers are purposely designed to avoid certain mutual coupling [12]–[18]. For example, [17], [18] use a capacitive coupler with long distance between the same side plates. It makes the coupler can be easily modeled as a series capacitor. In [19], only four mutual capacitances are considered while a pair of cross mutual capacitances are ignored. However, when system power density is taken into consideration, the system needs to be compact, which means the distance between each plate may not have sufficient freedom for placement. In this scenario, it is not acceptable to ignore certain coupling effects because all the mutual capacitors are comparable to each other. Therefore, having a general and simple coupling model for the capacitive coupler is very important for the development of CPT technology, based on which the circuit analysis and design can be significantly simplified.

Several research groups addressed the modeling issue [20], [21]. In these works, a pair of shunt capacitors and induced current sources, i.e., an induced current source (ICS) model, are used to represent the six mutual capacitors. This model simplifies six mutual capacitors and is helpful for system analysis. However, the shunt capacitance is coupling dependent, which causes troubles for resonance analysis under coupling variation [22]. For instance, if the equivalent shunt capacitor is designed for resonance, the achieved resonance frequency will naturally shift under coupling variation. In order to well deal with this issue, the circuit analysis based on the ICS model has to use superposition law or complicated transfer equation to derive the required resonance conditions [20], [23].

This paper develops an induced voltage source (IVS) model for the capacitive coupler. In this model, all the six mutual capacitive capacitors are represented through a pair of series self-capacitors and induced voltage sources. The self-capacitances are only determined by the area of plates and the relative position between the same-side plates, which are constant for most applications. A mutual capacitance or a coupling coefficient can represent all the coupling-dependent factors. This fascinating feature is exactly the same as that of the inductive power transfer (IPT) [24]. Based on this modeling approach, all the resonance analysis method for IPT can be directly introduced for CPT counterparts, and a uniform circuit theory can be developed. This paper will be arranged in five sections. Section two proposed the IVS model for CPT system. Finite-element analysis by Maxwell is used in section three to verify the coupling-independent property of the IVS model. Section four conducts the experiment to measure the self-capacitance in IVS model to evaluate the coupling-independent property. The last section gives a conclusion.

II. Induced Voltage Source (IVS) Model

A typical CPT system is shown in Fig. 1. Both TX and RX compensations are indispensable to boost the power transfer capability. The power is transferred from the TX plates of capacitive coupler (i.e., P_a and P_b) to the RX plates (i.e., P_c

978-1-7281-4829-8/20/$31.00 ©2020 IEEE

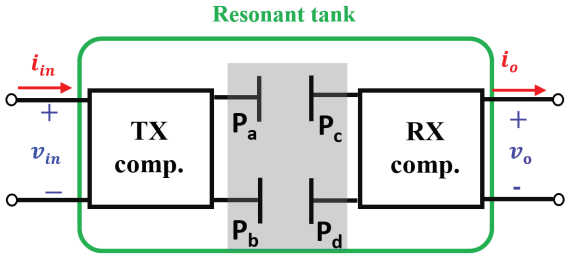

Fig. 1. The configuration of CPT system.

and P_d). A typical capacitive coupler is shown in Fig. 2(a). Since coupling exists between any two plates, there are six mutual capacitors (i.e., C_{ab}, C_{ac}, C_{ad}, C_{bc}, C_{bd}, and C_{cd}) in total (see Fig. 2(b)). In [20], the original six-capacitor model is represented by an induced current source model (see Fig. 2(c)) with the following equations:

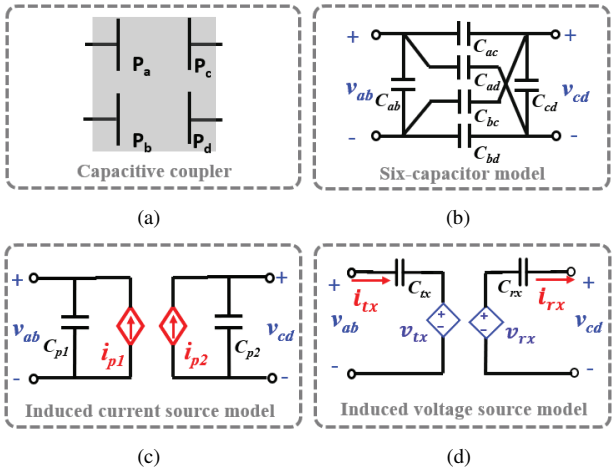

Fig. 2. Capacitive coupler and differnt circuit model (a) Typical capacitive coupler. (b) Six-capacitor model . (c) Induced current source model. (d) Induced voltage source model.

$$\begin{cases} C_{p1} = C_{ab} + \frac{(C_{ac}+C_{ad})(C_{bc}+C_{bd})}{C_{ac}+C_{ad}+C_{bc}+C_{bd}} \\ C_{p2} = C_{cd} + \frac{(C_{ac}+C_{bc})(C_{ad}+C_{bd})}{C_{ac}+C_{ad}+C_{bc}+C_{bd}} \\ C_{pm} = \frac{C_{bd}C_{ac}-C_{ad}C_{bc}}{C_{ac}+C_{ad}+C_{bc}+C_{bd}} \\ \boldsymbol{I_{p1}} = j\omega C_{pm} \cdot \boldsymbol{V_{cd}} \\ \boldsymbol{I_{p2}} = j\omega C_{pm} \cdot \boldsymbol{V_{ab}} \\ k = \frac{C_{pm}}{\sqrt{C_{p1}C_{p2}}} \end{cases} . \quad (1)$$

In this model, C_{p1} and C_{p2} are the equivalent shunt capacitors; C_{pm} is the mutual capacitor; k is the coupling coefficient; i_{p1} and i_{p2} are the induced current sources.

Considering the popularity of IVS model for IPT, it is very reasonable to accept the ICS model for CPT due to the circuit duality theory. It will be very engaging if mature IPT techniques [24]–[26] can be directly applied to its CPT counterpart since IPT technology is well-developed. However, the shunt capacitor (i.e., C_{p1} and C_{p2}) are coupling-dependent. Under coupling variation, if C_{p1} or C_{p2} are designed for resonance, the resonance frequency will naturally shift. Therefore, the existing topologies using ICS model have to use superposition law to analyze the resonance condition, and it is not very straightforward [9], [23].

The IVS model used for IPT coupler has two unique advantages. Firstly, the IPT coupler is modeled with fixed self-inductances that have clear physical meaning. Additionally, all the coupling-dependent factors are represented by a pair of induced voltage sources. Using this model, the achieved resonance frequency is naturally coupling-independent if the self-inductances in the IVS model are used for resonance. Because of these, the IVS model has been widely used for IPT coupler. Learning from IPT modeling experience, CPT coupler should be modeled with fixed self-capacitances and coupling-dependent induced sources. Apparently, the ICS model does not meet this requirement.

In this paper, the induced voltage source model is proposed for the capacitive coupler as shown in Fig. 2.(d). The voltage on each plate is defined as v_a, v_b, v_c, v_d respectively and Plate P_b is selected as the reference which means that $v_b = 0$, $v_{ab} = v_a$, $v_{cd} = v_c - v_d$. The input and output current of capacitive coupler is defined as i_{tx} and i_{rx} respectively. (2) can be derived from Kirchhoff's current equations

$$\begin{cases} \boldsymbol{I_{tx}}/(j\omega) = (C_{ab}+C_{ac}+C_{ad}) \cdot \boldsymbol{V_a} - C_{ac} \cdot \boldsymbol{V_c} - C_{14} \cdot \boldsymbol{V_d} \\ -\boldsymbol{I_{tx}}/(j\omega) = -C_{ab} \cdot \boldsymbol{V_a} - C_{bc} \cdot \boldsymbol{V_c} - C_{bd} \cdot \boldsymbol{V_d} \\ \boldsymbol{I_{rx}}/(j\omega) = C_{ac} \cdot \boldsymbol{V_a} - (C_{ac}+C_{bc}+C_{cd}) \cdot \boldsymbol{V_c} + C_{cd} \cdot \boldsymbol{V_d} \\ -\boldsymbol{I_{rx}}/(j\omega) = C_{ad} \cdot \boldsymbol{V_a} + C_{cd} \cdot \boldsymbol{V_c} - (C_{ad}+C_{bd}+C_{cd}) \cdot \boldsymbol{V_d} \end{cases} . \quad (2)$$

The relationship between across voltage of the capacitive coupler (v_{ab}, v_{cd}) and input and output current (i_{tx}, i_{rx}) can be derived from the equation (2). For example, the relationship between v_{ab}, i_{tx} and i_{rx} can be expressed by (3) by eliminating v_c and v_d. Similarly, the relationship between v_{cd}, i_{tx} and i_{rx} can be expressed by (4).

From (3) and (4), the self-capacitances (C_{tx},C_{rx}), the mutual capacitance (C_m),the induced voltage sources (V_{tx},V_{rx}) and coupling coefficient (k) in IVS model can be defined as (5). It is interesting to find that this new define coupling coefficient k is exactly the same as that of (1).

Based on the two-port network theory, the ICS model and IVS model for capacitive coupler are interconvertible. For the ICS model, is has

$$\begin{bmatrix} \boldsymbol{I_{tx}} \\ \boldsymbol{I_{rx}} \end{bmatrix} = \begin{bmatrix} j\omega C_{p1} & -j\omega C_{pm} \\ j\omega C_{p2} & j\omega C_{pm} \end{bmatrix} \begin{bmatrix} \boldsymbol{V_{ab}} \\ \boldsymbol{V_{cd}} \end{bmatrix} . \quad (6)$$

Similarly, for the IVS model, it has

$$\begin{bmatrix} \boldsymbol{V_{ab}} \\ \boldsymbol{V_{cd}} \end{bmatrix} = \begin{bmatrix} \frac{1}{j\omega C_{tx}} & \frac{1}{j\omega C_m} \\ -\frac{1}{j\omega C_m} & \frac{1}{j\omega C_{rx}} \end{bmatrix} \begin{bmatrix} \boldsymbol{I_{tx}} \\ \boldsymbol{I_{rx}} \end{bmatrix} . \quad (7)$$

The relationship between C_{tx}, C_{rx}, C_m in the IVS model and C_{p1}, C_{p2}, C_m in the ICS model can be derived from (6) and (7).

$$\boldsymbol{V_{ab}} = \frac{1}{j\omega[C_{ab} + \frac{C_{ac}C_{ad}(C_{bc}+C_{bd})+C_{bc}C_{bd}(C_{ac}+C_{ad})+C_{cd}(C_{ac}+C_{ad})(C_{bc}+C_{bd})}{(C_{ac}+C_{bc})(C_{ad}+C_{bd})+C_{cd}(C_{ac}+C_{ad}+C_{bc}+C_{bd})}]} \cdot \boldsymbol{I_{tx}}$$

$$+ \frac{1}{j\omega[\frac{C_{ab}C_{cd}(C_{ac}+C_{ad}+C_{bc}+C_{bd})+C_{cd}(C_{ac}+C_{ad})(C_{bc}+C_{bd})+C_{ab}(C_{ac}+C_{bc})(C_{ad}+C_{bd})+C_{ac}C_{ad}(C_{bc}+C_{bd})+C_{bc}C_{bd}(C_{ac}+C_{ad})}{C_{ac}C_{bd}-C_{ad}C_{bc}}]} \cdot \boldsymbol{I_{rx}} \tag{3}$$

$$\boldsymbol{V_{cd}} = \frac{-1}{j\omega[\frac{C_{ab}C_{cd}(C_{ac}+C_{ad}+C_{bc}+C_{bd})+C_{cd}(C_{ac}+C_{ad})(C_{bc}+C_{bd})+C_{ab}(C_{ac}+C_{bc})(C_{ad}+C_{bd})+C_{ac}C_{ad}(C_{bc}+C_{bd})+C_{bc}C_{bd}(C_{ac}+C_{ad})}{C_{ac}C_{bd}-C_{ad}C_{bc}}]} \cdot \boldsymbol{I_{tx}}$$

$$+ \frac{1}{j\omega[C_{cd} + \frac{C_{ad}C_{bc}(C_{ac}+C_{bd})+C_{ac}C_{bd}(C_{ad}+C_{bc})+C_{ab}(C_{ac}+C_{ad})(C_{bc}+C_{bd})}{(C_{ac}+C_{bc})(C_{ad}+C_{bd})+C_{cd}(C_{ac}+C_{ad}+C_{bc}+C_{bd})}]} \cdot \boldsymbol{I_{rx}} \tag{4}$$

$$\begin{cases} C_{tx} = C_{ab} + \frac{C_{ac}C_{ad}(C_{bc}+C_{bd})+C_{bc}C_{bd}(C_{ac}+C_{ad})+C_{cd}(C_{ac}+C_{ad}+C_{bc}+C_{bd})}{(C_{ac}+C_{bc})(C_{ad}+C_{bd})+C_{cd}(C_{ac}+C_{ad}+C_{bc}+C_{bd}} \\ C_{rx} = C_{cd} + \frac{C_{ad}C_{bc}(C_{ac}+C_{bd})+C_{ac}C_{bd}(C_{ad}+C_{bc})+C_{ab}(C_{ac}+C_{ad}+C_{bc}+C_{bd})}{(C_{ac}+C_{bc})(C_{ad}+C_{bd})+C_{cd}(C_{ac}+C_{ad}+C_{bc}+C_{bd})} \\ C_m = \frac{C_{ab}C_{cd}(C_{ac}+C_{ad}+C_{bc}+C_{bd})+C_{cd}(C_{ac}+C_{ad})(C_{bc}+C_{bd})+C_{ab}(C_{ac}+C_{bc})(C_{ad}+C_{bd})+C_{ac}C_{ad}(C_{bc}+C_{bd})+C_{bc}C_{bd}(C_{ac}+C_{ad})}{C_{ac}C_{bd}-C_{ad}C_{bc}} \\ \boldsymbol{V_{tx}} = \frac{1}{j\omega C_m} \cdot \boldsymbol{I_{rx}} \\ \boldsymbol{V_{rx}} = -\frac{1}{j\omega C_m} \cdot \boldsymbol{I_{rx}} \\ k = \frac{\sqrt{C_{tx}C_{rx}}}{C_m} = \frac{C_{pm}}{\sqrt{C_{p1}C_{p2}}} \end{cases} . \tag{5}$$

$$\begin{cases} C_{tx} = \frac{C_{p1}C_{p2}-C_{pm}C_{pm}}{C_{p2}} \\ C_{rx} = \frac{C_{p1}C_{p2}-C_{pm}C_{pm}}{C_{p1}} \\ C_m = \frac{C_{p1}C_{p2}-C_{pm}C_{pm}}{C_{pm}} \end{cases} . \tag{8}$$

From the mathematical point of view, it is difficult to determine whether C_{tx} and C_{rx} are coupling dependent or not. Therefore, this problem should be analyzed from a circuit standpoint. Actually, C_{tx} is the input capacitance when $v_{tx} = 0$, and this feature is exactly the same with that of the self-inductance in an IPT system i.e., the self-inductance of TX side is achieved by opening the RX side coil (having $i_{rx} = 0$) or removing the RX side coil (having $k = 0$). The physical meaning of the self-capacitor C_{tx} can be obtained by introducing this IPT modeling experience to CPT and it is the capacitor between P_a and P_b when removing the RX side plates(i.e., P_c and P_d). This capacitance is only related to the TX side plates, to be more specific, the relative position of P_a and P_b and the area of P_a and P_b, which are fixed for CPT applications. It should be noted that the self-capacitor C_{tx} is not C_{ab} in Fig. 2. In the six-capacitor model, C_{ab} is a only part of overall equivalent capacitor between P_a and P_b. As shown in (5), $C_{tx} = C_{ab}$ only when the RX plates are removed. It should be noticed that C_{ab} cannot be directly measured when the RX plates exist, and its value is shift under coupling variation. However, C_{tx} is fixed and has clear physical meaning. This definition is exactly the same as that of an IPT system. Based on this modeling approach, most well-developed IPT techniques can be directly applied to CPT.

III. SIMULATION VERIFICATION

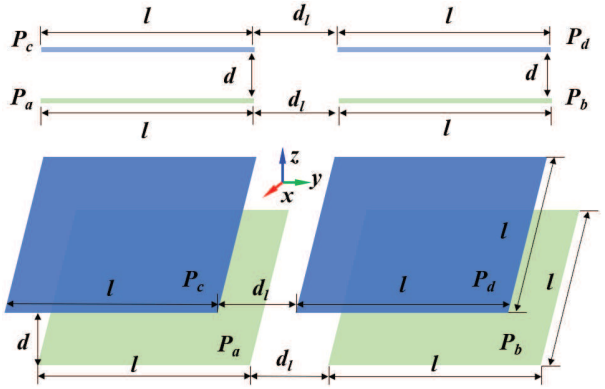

Fig. 3. Dimensions of the capacitive coupler.

The simulation is conducted by maxwell to verify the proposed IVS model. Four identical square plates are used to form a capacitive coupler. Six mutual capacitors in a four-plate coupler are directly obtained from the simulation and all the other capacitances (i.e. C_{p1}, C_{p2}, C_{pm} in ICS model and C_{tx}, C_{rx}, C_m in IVS model) are calculated based on (1) and (5).

Fig. 3 shows the front view and three-dimensional view of capacitive coupler to illustrate the structure and dimensions

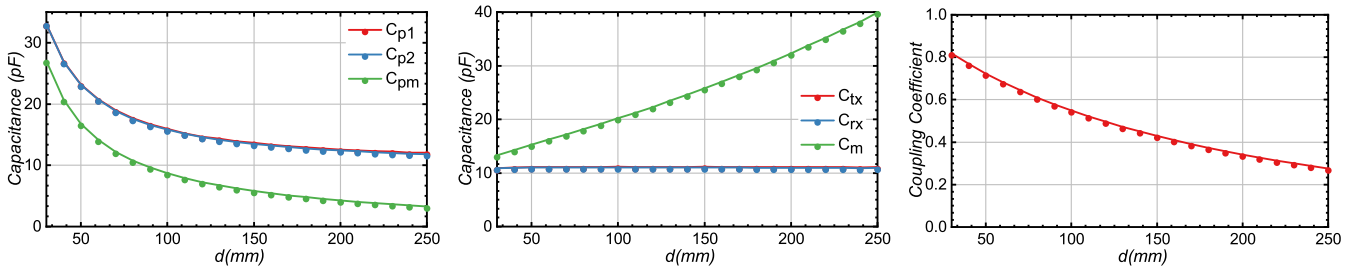

(a) (b) (c)

Fig. 4. Parameters of capacitive coupler at different d. (a) C_{p1}, C_{p2}, C_{pm} in the ICS model. (b) C_{tx}, C_{rx}, C_m in the IVS model. (c) The coupling coefficient k.

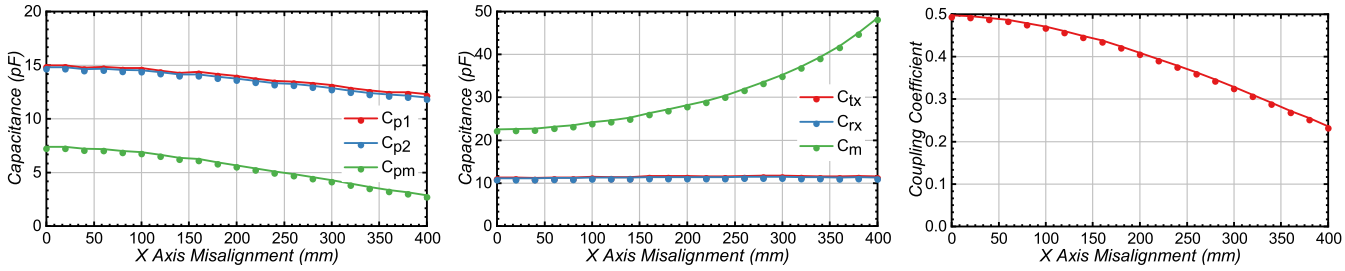

(a) (b) (c)

Fig. 5. Parameters of capacitive coupler at different X axis misalignment. (a) C_{p1}, C_{p2}, C_{pm} in the ICS model. (b) C_{tx}, C_{rx}, C_m in the IVS model. (c) The coupling coefficient k.

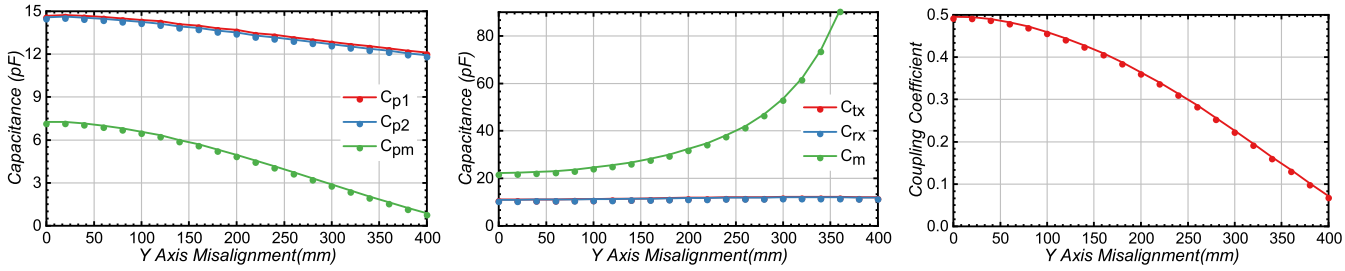

(a) (b) (c)

Fig. 6. Parameters of capacitive coupler at different Y axis misalignment. (a) C_{p1}, C_{p2}, C_{pm} in the ICS model. (b) C_{tx}, C_{rx}, C_m in the IVS model. (c) The coupling coefficient k.

of the plates. The plates are symmetric from the TX side to the RX side. Plates P_a and P_b are placed at the TX side, at the same time, plates P_c and P_d are placed at the RX side. The length of four plates is l, the distance of $P_a - P_c$ and $P_b - P_d$ is d, the distance of $P_a - P_b$ and $P_c - P_d$ is d_l. In the simulation, the default value of l, d, d_l is setted as $400mm$, $120mm$, $260mm$ respectively.

In the first case, d changes from $30mm$ to $220mm$ with $10mm$ step size and others parameters are fixed. The six mutual capacitances change with d are shown in Table I. C_{p1}, C_{p2}, C_{pm} in the ICS model, C_{tx}, C_{rx}, C_m in the IVS model and the capacitive coefficient k at different d are shown in Fig. 4. It clearly shows that the self-capacitances, C_{tx} and C_{rx}, in the IVS model are fixed and the increasing distance d only leads to a increasing C_m or decreasing k. But it should be noted that, the shunt capacitances C_{p1} and C_{p2} in the ICS model are coupling-dependent.

In the second case, there is an X-axis misalignment of the RX side (P_c and P_d). The six mutual capacitances change with x are shown in Table II. C_{p1}, C_{p2}, C_{pm} in the ICS model, C_{tx}, C_{rx}, C_m in the IVS mode and and the coupling coefficient k are shown in Fig. 5. Similar to case one, the results show the self-capacitances C_{tx} and C_{rx} is fixed and the coupling-dependent factors are represented by the coupling coefficient k, which is the same with case one. The simulation results of the third case are shown in Table III and Fig. 6 are similar with the second case. Therefore, the self-capacitances in the IVS model are coupling-independent.

TABLE I
SIX MUTUAL CAPACITORS AT DIFFERENT d.

d (mm)	C_{ab} (pF)	C_{ac} (pF)	C_{ad} (pF)	C_{cd} (pF)	C_{bd} (pF)	C_{bc} (pF)
30	3.17	56.88	2.84	3.14	56.90	2.84
40	3.30	44.26	2.94	3.26	44.21	2.94
50	3.43	36.53	3.02	3.37	36.58	3.02
60	3.54	31.36	3.09	3.47	31.39	3.09
70	3.62	27.54	3.15	3.55	27.55	3.14
80	3.73	24.73	3.20	3.64	24.72	3.20
90	3.82	22.49	3.24	3.73	22.50	3.26
100	3.93	20.74	3.30	3.80	20.75	3.31
110	3.99	19.17	3.34	3.88	19.17	3.34
120	4.06	17.89	3.38	3.96	17.90	3.38
130	4.17	16.89	3.43	4.04	16.89	3.43
140	4.24	15.95	3.47	4.11	15.96	3.47
150	4.33	15.15	3.51	4.18	15.15	3.50
160	4.40	14.42	3.54	4.24	14.41	3.53
170	4.46	13.76	3.56	4.32	13.77	3.57
180	4.54	13.19	3.59	4.37	13.19	3.60
190	4.61	12.68	3.62	4.43	12.67	3.63
200	4.66	12.19	3.65	4.51	12.19	3.66
210	4.74	11.76	3.68	4.56	11.78	3.68
220	4.80	11.37	3.70	4.62	11.38	3.70
230	4.87	11.00	3.72	4.67	11.01	3.73
240	4.87	10.62	3.74	4.73	10.62	3.73
250	4.99	10.37	3.77	4.78	10.37	3.77

TABLE II
SIX MUTUAL CAPACITORS AT X MISALIGNMENT CONDITIONS.

X (mm)	C_{ab} (pF)	C_{ac} (pF)	C_{ad} (pF)	C_{cd} (pF)	C_{bd} (pF)	C_{bc} (pF)
400	5.55	9.64	3.89	5.23	9.62	3.89
380	5.46	10.16	3.88	5.15	10.13	3.86
360	5.29	10.55	3.82	5.06	10.57	3.83
340	5.20	11.09	3.80	4.98	11.09	3.80
320	5.15	11.70	3.79	4.91	11.65	3.77
300	5.12	12.33	3.78	4.82	12.31	3.76
280	5.03	12.87	3.75	4.76	12.91	3.74
260	4.91	13.42	3.72	4.70	13.40	3.72
240	4.78	13.83	3.66	4.58	13.83	3.68
220	4.73	14.41	3.65	4.50	14.40	3.65
200	4.69	14.95	3.63	4.45	14.99	3.64
180	4.61	15.49	3.62	4.38	15.55	3.61
160	4.56	16.09	3.60	4.32	16.08	3.59
140	4.39	16.28	3.53	4.23	16.28	3.53
120	4.34	16.77	3.50	4.20	16.79	3.53
100	4.35	17.26	3.50	4.13	17.29	3.52
80	4.25	17.51	3.48	4.08	17.49	3.46
60	4.22	17.83	3.45	4.04	17.82	3.46
40	4.13	17.89	3.42	4.01	17.85	3.42
20	4.17	18.19	3.44	4.01	18.19	3.42
0	4.16	18.21	3.42	3.99	18.22	3.42

TABLE III
SIX MUTUAL CAPACITORS AT Y MISALIGNMENT CONDITIONS.

Y (mm)	C_{ab} (pF)	C_{ac} (pF)	C_{ad} (pF)	C_{cd} (pF)	C_{bd} (pF)	C_{bc} (pF)
400	4.26	8.74	11.53	4.07	8.73	4.13
380	4.23	9.28	10.94	4.05	9.26	4.06
360	4.20	9.85	10.31	4.03	9.84	4.00
340	4.19	10.43	9.73	4.01	10.40	3.92
320	4.16	11.01	9.10	3.99	11.00	3.85
300	4.14	11.62	8.52	3.98	11.59	3.77
280	4.13	12.22	7.95	3.97	12.19	3.70
260	4.11	12.81	7.38	3.96	12.80	3.64
240	4.13	13.40	6.90	3.94	13.38	3.57
220	4.09	13.95	6.40	3.94	13.91	3.48
200	4.13	14.57	6.00	3.94	14.55	3.44
180	4.10	15.07	5.57	3.93	15.03	3.37
160	4.10	15.62	5.20	3.94	15.58	3.32
140	4.08	16.01	4.84	3.93	16.01	3.27
120	4.11	16.54	4.57	3.94	16.52	3.24
100	4.09	16.91	4.29	3.94	16.88	3.21
80	4.09	17.27	4.04	3.95	17.24	3.20
60	4.08	17.54	3.83	3.96	17.53	3.22
40	4.08	17.77	3.64	3.96	17.77	3.25
20	4.08	17.92	3.51	3.97	17.93	3.30
0	4.06	17.89	3.38	3.96	17.90	3.38

IV. EXPERIMENT

The experiment setup is shown in Fig. 7. The self-capacitances ,C_{tx} and C_{rx}, in IVS model and the shunt capacitances, C_{p1} and C_{p2}, in ICS model are measured by a vector network analyzer (N9915A, Keysight Inc) to verify the proposed IVS model. Fig. 8 shows that the self-capacitances ,C_{tx} and C_{rx}, in IVS model are fixed, which means the experiment results are consistent with the simulation results.

Fig. 7. Experimental plates setup.

V. CONCLUSION AND FUTURE WORKS

This paper proposes an induced voltage source model for the capacitive coupler. In this model, the original six coupling-dependent capacitors of a four-plate coupler can be equiv-

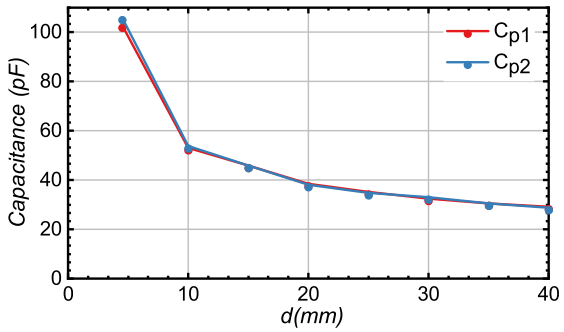

(a)

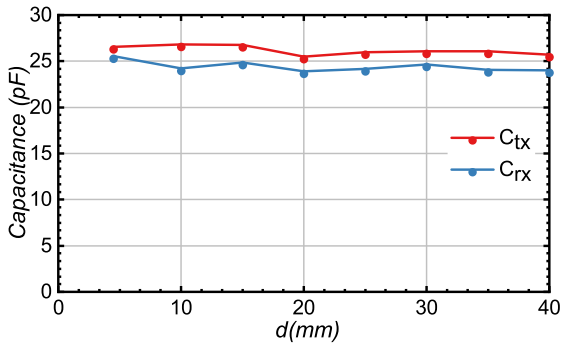

(b)

Fig. 8. Experimental results. (a) C_{p1}, C_{p2} in the ICS model. (b) C_{tx}, C_{rx} in the IVS model.

alently represented by two self-capacitances and a pair of induced voltage sources. The attractive point of this model is that self-capacitances are coupling-independent, which is the same as that of an IPT coupler. The simulation and experiment results verify the proposed IVS model for the capacitive coupler. Future work will focus on the investigation of the existing topologies and the development of new compensations based on IVS model.

REFERENCES

[1] M. Fu, T. Zhang, C. Ma, and X. Zhu, "Efficiency and optimal loads analysis for multiple-receiver wireless power transfer systems," *IEEE Trans. Microw. Theory Techn.*, vol. 63, no. 3, pp. 801–812, 2015.

[2] J. Feng, Q. Li, F. C. Lee, and M. Fu, "Transmitter Coils Design for Free-Positioning Omnidirectional Wireless Power Transfer System," *IEEE Trans. Ind. Inf.*, vol. 15, no. 8, pp. 4656–4664, Aug. 2019.

[3] C. Liao, J. Li, and S. Li, "Design of LCC impedance matching circuit for wireless power transfer system under rectifier load," *CPSS Transactions on Power Electronics and Applications*, vol. 2, no. 3, pp. 237–245, Sep. 2017.

[4] B. Regensburger, S. Sinha, A. Kumar, J. Vance, Z. Popovic, and K. K. Afridi, "Kilowatt-scale large air-gap multi-modular capacitive wireless power transfer system for electric vehicle charging," in *2018 IEEE Applied Power Electronics Conference and Exposition (APEC)*. San Antonio, TX, USA: IEEE, Mar. 2018, pp. 666–671.

[5] A. Kumar, S. Sinha, A. Sepahvand, and K. K. Afridi, "Improved Design Optimization for High-Efficiency Matching Networks," *IEEE Trans. Power Electron.*, vol. 33, no. 1, pp. 37–50, Jan. 2018.

[6] M. Fu, Z. Tang, and C. Ma, "Analysis and optimized design of compensation capacitors for a megahertz wpt system using full-bridge rectifier," *IEEE Trans. Ind. Inf.*, vol. 15, no. 1, pp. 95–104, 2018.

[7] S. Y. R. Hui, "Past, present and future trends of non-radiative wireless power transfer," *CPSS Transactions on Power Electronics and Applications*, vol. 1, no. 1, pp. 83–91, Dec. 2016.

[8] D. J. Graham, J. A. Neasham, and B. S. Sharif, "Investigation of Methods for Data Communication and Power Delivery Through Metals," *IEEE Trans. Ind. Electron.*, vol. 58, no. 10, pp. 4972–4980, Oct. 2011.

[9] F. Lu, H. Zhang, H. Hofmann, and C. Mi, "A Double-Sided LCLC-Compensated Capacitive Power Transfer System for Electric Vehicle Charging," *IEEE Trans. Power Electron.*, vol. 30, no. 11, pp. 6011–6014, Nov. 2015.

[10] C. Chen, C. Li, C. Liao, and L. Wang, "Parameter identification of capacitive power transfer system based on spectrum analysis," *CPSS Transactions on Power Electronics and Applications*, vol. 3, no. 3, pp. 181–186, Sep. 2018.

[11] E. Abramov, I. Zeltser, and M. M. Peretz, "A network-based approach for modeling resonant capacitive wireless power transfer systems," *CPSS Transactions on Power Electronics and Applications*, vol. 4, no. 1, pp. 19–29, Mar. 2019.

[12] J. Dai, S. Hagen, D. C. Ludois, and I. P. Brown, "Synchronous Generator Brushless Field Excitation and Voltage Regulation via Capacitive Coupling Through Journal Bearings," *IEEE Trans. on Ind. Applicat.*, vol. 53, no. 4, pp. 3317–3326, Jul. 2017.

[13] D. C. Ludois, J. K. Reed, and K. Hanson, "Capacitive Power Transfer for Rotor Field Current in Synchronous Machines," *IEEE Trans. Power Electron.*, vol. 27, no. 11, pp. 4638–4645, Nov. 2012.

[14] J. Dai and D. C. Ludois, "Single active switch power electronics for kilowatt scale capacitive power transfer," *IEEE J. Emerg. Sel. Topics Power Electron.*, vol. 3, no. 1, pp. 315–323, March 2015.

[15] Y. Su, S. Xie, A. P. Hu, C. Tang, W. Zhou, and L. Huang, "Capacitive power transfer system with a mixed-resonant topology for constant-current multiple-pickup applications," *IEEE Trans. Power Electron.*, vol. 32, no. 11, pp. 8778–8786, Nov 2017.

[16] F. Lu, H. Zhang, H. Hofmann, and C. Mi, "A CLLC-compensated high power and large air-gap capacitive power transfer system for electric vehicle charging applications," in *2016 IEEE Applied Power Electronics Conference and Exposition (APEC)*. Long Beach, CA, USA: IEEE, Mar. 2016, pp. 1721–1725.

[17] L. Huang, A. P. Hu, A. K. Swain, and Y. Su, "Z-Impedance Compensation for Wireless Power Transfer Based on Electric Field," *IEEE Trans. Power Electron.*, vol. 31, no. 11, pp. 7556–7563, Nov. 2016.

[18] M. P. Theodoridis, "Effective Capacitive Power Transfer," *IEEE Trans. Power Electron.*, vol. 27, no. 12, pp. 4906–4913, Dec. 2012.

[19] L. Huang and A. Hu, "Defining the mutual coupling of capacitive power transfer for wireless power transfer," *Electronics Letters*, vol. 51, no. 22, pp. 1806–1807, Oct. 2015.

[20] H. Zhang, F. Lu, H. Hofmann, W. Liu, and C. Mi, "A 4-Plate Compact Capacitive Coupler Design and LCL-Compensated Topology for Capacitive Power Transfer in Electric Vehicle Charging Applications," *IEEE Trans. Power Electron.*, pp. 1–1, 2016.

[21] C. Liu, A. P. Hu, and M. Budhia, "A generalized coupling model for Capacitive Power Transfer systems," in *IECON 2010 - 36th Annual Conference on IEEE Industrial Electronics Society*. Glendale, AZ, USA: IEEE, Nov. 2010, pp. 274–279.

[22] H. Zhang, F. Lu, H. Hofmann, and C. Mi, "A loosely coupled capacitive power transfer system with LC compensation circuit topology," in *2016 IEEE Energy Conversion Congress and Exposition (ECCE)*. Milwaukee, WI, USA: IEEE, Sep. 2016, pp. 1–5.

[23] F. Lu, H. Zhang, H. Hofmann, and C. C. Mi, "A Double-Sided LC-Compensation Circuit for Loosely Coupled Capacitive Power Transfer," *IEEE Trans. Power Electron.*, vol. 33, no. 2, pp. 1633–1643, Feb. 2018.

[24] R. He, P. Zhao, M. Fu, Y. Liu, H. Wang, and J. Liang, "Decomposition and Synthesis of High-Order Compensated Inductive Power Transfer Systems for Improved Output Controllability," *IEEE Trans. Microw. Theory Techn.*, pp. 1–10, 2019.

[25] M. Fu, H. Yin, X. Zhu, and C. Ma, "Analysis and Tracking of Optimal Load in Wireless Power Transfer Systems," *IEEE Trans. Power Electron.*, vol. 30, no. 7, pp. 3952–3963, Jul. 2015.

[26] S. Li, W. Li, J. Deng, T. D. Nguyen, and C. C. Mi, "A Double-Sided LCC Compensation Network and Its Tuning Method for Wireless Power Transfer," *IEEE Trans. Veh. Technol.*, vol. 64, no. 6, pp. 2261–2273, Jun. 2015.